Conf-9502126--1

LA-UR- 95- 116

Title: Analysis of Surfaces, Films and Multilayers by Resonant Laser Ablation

Author(s): T. M. Allen, C. H. Smith, P. B. Kelly, J. E. Anderson, G. C. Eiden, A. W. Garrett, C. G. Gill, P. H. Hemberger, and N. S. Nogar

Submitted to: Proceedings of SPIE OE LASE '95 Meeting, San Jose, CA February 4-10, 1995

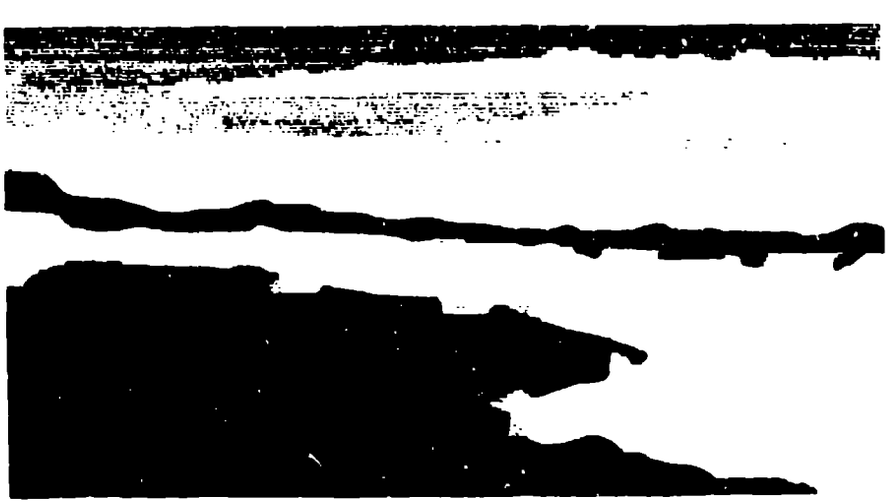

Los Alamos
NATIONAL LABORATORY

Form No 836 R5
ST 2629 10/91

DISTRIBUTION OF THIS DOCUMENT IS UNLIMITED

Analysis of Surfaces, Films and Multilayers by Resonant Laser Ablation

T. M. Allen, C. H. Smith and P. B. Kelly
Department of Chemistry
University of California, Davis
Davis, California 95616

J. E. Anderson, G. C. Eiden*, A.W. Garrett, C. G. Gill,
P. H. Hemberger and N. S. Nogar
CST-1, MS J565
Los Alamos National Laboratory
Los Alamos, New Mexico 87545
*Current Address: P8-08, PNL
Richland, Washington 99352

ABSTRACT

In this manuscript we review briefly the history of Resonant Laser Ablation (RLA), and discuss some current ideas regarding sample preparation, laser parameters, and mechanisms. We also discuss current applications including spectral analysis of trace components, depth profiling of thin films and multilayer structures, and the use of RLA with the Ion Trap Mass Spectrometer (ITMS).

1. INTRODUCTION

Ever since the first report of laser action, it has been recognized that laser ablation (evaporation/volatilization) may provide a useful sampling mechanism for chemical analysis[1-4]. The potentially high heating rates (10^{10}K/sec) can produce gas phase plumes, amenable to analysis, which have compositions representative of the sampled surface[5]. With the recent resurgence in the popularity of multiplex mass spectrometry (ToF[6], ITMS[7] and FTICR[8]), laser ablation is rapidly gaining popularity as a method of sample introduction for mass spectrometry.

Since its original description, numerous research papers and review articles have appeared on various aspects of laser mass spectrometry. Several attributes are characteristic of laser mass spectrometry: 1) no background is introduced due to bulk heating of the sample; 2) spatial resolution can be very good, limited only by diffraction of the incident beam (typically ~1 μm in diameter) and, at high fluxes, cratering of the surface (typically ~10 μm); 3) little sample preparation is needed; 4) sensitivity is excellent, and the

detection limit frequently falls in the femtogram to attogram (absolute) or sub-parts-per-billion range.

While most laser ablation/mass spectrometry has been performed with fixed frequency lasers operating at relatively high intensities/fluences ($\geq 10^8$ W/cm^2, ≥ 1 J/cm^2), there has been some recent interest in the use of tunable lasers to enhance the ionization yield of selected components in an analytical sample. This process has been termed resonant laser ablation (RLA)[9-11], and typically relies on irradiation of a sample in a mass spectrometer with modest intensity laser pulses tuned to a one- or two-photon resonant transition in the analyte of interest. Recently, Ledingham's group[9-14] and our own[15-17] have begun systematic study of the process on a variety of materials.

Potential advantages of RLA include: 1) simplification of the mass spectrum, by enhancement of signal from the analyte of interest; 2) improvement of the absolute detection limits by improving the ionization efficiency, and 3) improvement in relative sensitivity. RLA tends to produce higher mass resolution because of minimal spatial spread in the ion source and small space charge effects. In this manuscript we present a survey of RLA attributes and applications, including laser spot-size dependence, and the effects of polarization, and surface finish. We also describe the use of RLA for the analysis of thin films, and as an ion source for ion trap mass spectrometry. The use of RLA for spectroscopy of small or very dilute samples is also noted. In addition, we discuss mechanisms that describe these results.

2. Experimental

2.1 Lasers and Optics

Several optical sources were used in these experiments. Typically, one of several excimer-laser pumped dye lasers was used to produce laser pulses @ 10 Hz having the following characteristics: 1-5 mJ/pulse; ~12 nsec pulse duration; spectral output 440-480 nm, with a spectral bandwidth of 0.05, 0.3 or 0.7 cm^{-1}. Few gross differences were noted with the results obtained from these various lasers, though in general, the narrower bandwidth lasers produced the largest signal and the smallest background.

The output from the dye laser passed through a variety of beam-steering optics, through a variable attenuator, a polarization rotator, and a quartz focusing lens (15 cm) mounted on a precision 5-axis positioner. Beam energy could be monitored directly, by insertion of an energy meter in the beam line, or indirectly, by the use of calibrated photodiodes that viewed both a reflection from the incident beam, and the residual transmitted beam reflected from the sample surface and out of the vacuum can. Typical incident pulse energies fell in the range 1-40 μJ. Pulse size and shape could be monitored on a shot-to-shot basis with a CCD camera mounted on a parallel beam line, and monitored with beam-analysis software.

Typical laser spots at the sample surface were round, with a FWHM diameter of 110 μm. Since the beam was projected on the surface at an angle 11° from grazing incidence, the projected spot on the surface was ≈ 110 μm x 550 μm.

In other experiments, a nitrogen laser pumped dye laser was used. This apparatus produced a maximum pulse energy of 85 μJ in a pulse of ≈3 nsec duration, and a bandwidth of 2 cm^{-1}. The beam was apertured, and delivered to the sample with a 20 cm focusing lens, again mounted in a precision 5-axis optical stage.

2.2 Mass Spectrometers & Detection

Most of the data reported here was obtained with two time-of-flight (ToF) mass spectrometer systems, a 0.4 m linear ToF, and a 1 m reflecting ToF. The former was pumped to a base pressure ≈ 1 x 10^{-7} Torr, with a potential in the extraction region of 500 V/cm, and equipped with a channel electron multiplier for detection; resolution was typically ≈200 (m/Δm). The latter was pumped to a base pressure ≈ 1 x 10^{-9} Torr, with a potential in the extraction region of 1000 V/cm, and equipped with a channel plate detector; resolution for this instrument was ≈1200 (m/Δm). In either case, signal was passed through an impedance matching preamplifier, and then to a transient recorder (for ToF measurements) or to a gated integrator (for time-dependent or spectral measurements). Data was transferred to a microcomputer for storage and subsequent data analysis.

Some experiments were performed with an ion trap mass spectrometer (ITMS). The ITMS was mounted inside a 1 m diameter vacuum can capable of base pressures ≤ 10^{-8} Torr. The laser beam was focused (65 cm lens) through a 2.5 mm hole in the ring electrode of a Finnigan ion trap mass spectrometer as described previously, producing a roughly circular gaussian spot on the target, which was inserted trough the opposite side of the ring electrode. Helium was used as a buffer gas at an uncorrected gauge pressure of 1-2 x 10^{-5} Torr for all experiments. The scan function utilized a ramped rf potential, as described previously, to improve signal levels.[18] The laser was triggered by a digital delay generator that was triggered synchronously with the scan function at a zero crossing of the RF generator as the RF began to rise. The ions were stored for 10 to 15 msec after desorption before the analytical ramp.

2.3 Samples, Preparation and Analysis

Samples were mounted on a rotatable push/pull vacuum feedthrough, with the face of the sample mounted flush with the repeller plate of the ToF extraction region. Samples consisted of 1/2" disks of bulk material (typically copper, bronze or stainless steel), NIST standard reference materials, (C1154a, also machined to 1/2" diameter disks), copper-coated silicon

wafers, or multilayer dielectric structures. The bulk and standard reference materials were used both polished to a mirror finish and with a roughened surface.

Following exposure to the laser beam, the surfaces could examined by both optical microscopy and by a surface profilometer. Optical microscopy was used routinely to measure the size of the surface figure etched by the laser beam, typically 20 x 60 μm. Selected spots were also examined with a stylus profilometer, to measure the depth of the etch, and to confirm the spot size measured by optical microscopy.

3. Results & Discussion

3.1 General Observations.

Resonant laser ablation is believed to be a multistep process. The leading (temporal) edge of the laser pulse interacts with the solid surface to produce a relatively low density gas phase plume[15] In our experiments we estimate that the removal rate is ~0.001 monolayer/shot; after 5 nsec, and assuming a plume velocity of 1 x 10^5 cm/sec, this corresponds to a density of 3 x 10^{16} cm^{-3}, or an effective pressure ~ 10^{-3} Torr at standard temperature. The trailing edge of the laser pulse interacts with the gas-phase plume, via a resonant excitation/ionization process, to selectively generate ions. Figure 1 shows a

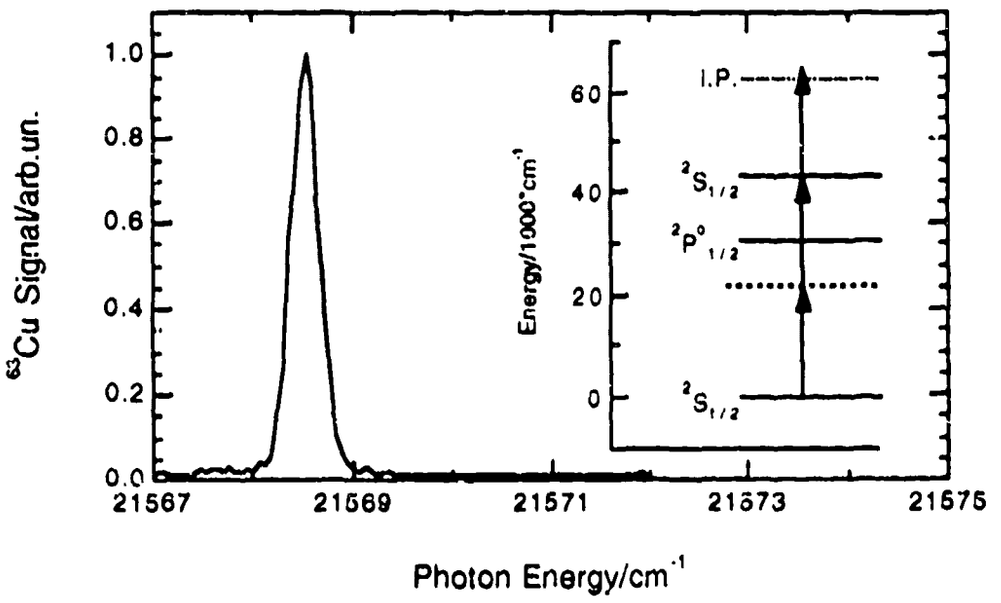

Figure 1 shows the resonant spectrum of copper from a copper film. The FWHM of the spectral feature is 0.35 cm^{-1}, which is laser linewidth limited.

resonant excitation spectrum for the copper $(3d^{10}5s)\ ^2S_{1/2} \leftarrow (3d^{10}4s)\ ^2S_{1/2}$ "2+1" (photons to resonance + photons to ionize) ionization process. Also shown is a simplified energy level diagram, indicating the relevant energy levels.

Figure 2 shows RLA mass spectra generated from the NIST SRM. Each spectrum corresponds to irradiation of the surface at a different wavelength, corresponding to a resonant "2+1" ionization process for the labeled element: chromium, copper or tin. Several features are worth noting. First, signal was obtained with low pulse energies, corresponding to fluences ≤50 mJ/cm^2. The observation of trace components at very low laser intensities is a significant virtue of this process; this sensitivity is due both to the resonant nature of the ionization process, and to the excellent overlap of the vaporized sample with the ionizing laser beam. Second, virtually no signal due to the bulk material (Fe) was observed. In more careful experiments, we have demonstrated selectivity in ionization of the target analyte vs. the bulk material of ≥10^5:1. In spite of this, a persistent signal due to sodium (3.4 µsec) and potassium (4.4 µsec) is observed in all of these spectra. These components are observed here, and in other work, presumably because of their high volatility, low ionization potential and presence on the surface as ionic compounds. They are thus easily vaporized, and ionized, by low-order non-resonant multiphoton processes.

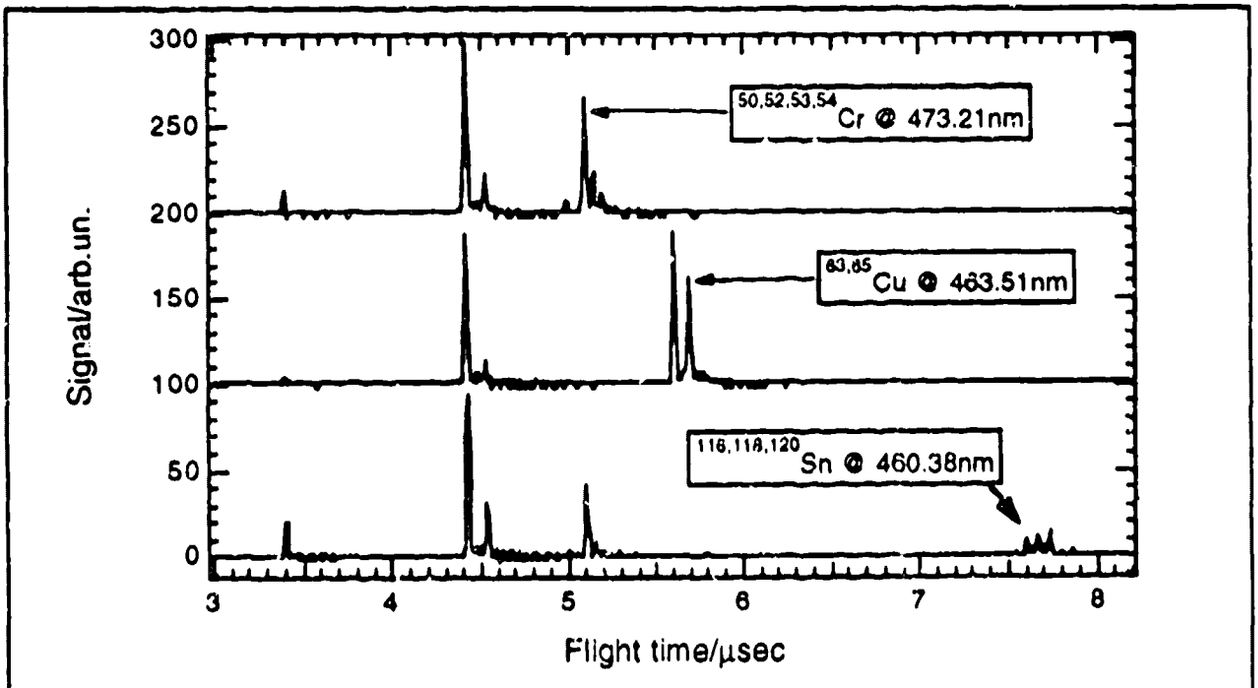

Figure 2 shows the ability to analyze different components from a complex mixture simply by change resonant excitation wavelengths. All resonant ionization is due to "2+1" ionization processes.

3.2 Laser Spot Size.

As noted earlier, we monitor both the laser spatial profile (on a parallel beam line), with a CCD camera and the damaged spot size on the sample surface. A typical experiment of the optical beam size yields a measured beam size (FWHM) of 110 μm (round), while measured spot size on surface is 20 μm x 60 μm (out-of-round due to the due to 11-degree projection on surface), as shown in Figure 3. This discrepancy is presumably due to the high order of the RLA process. We have previously measured the intensity (I) dependence of the signal (S) to scale as $S \propto I^n$, with $6 \leq n \leq 12$[15]. For a gaussian beam having a FWHM diameter of 100 μm, the corresponding [gaussian^{10}] beam will have a FWHM diameter of ≈25 μm, very close to our observed spot size.

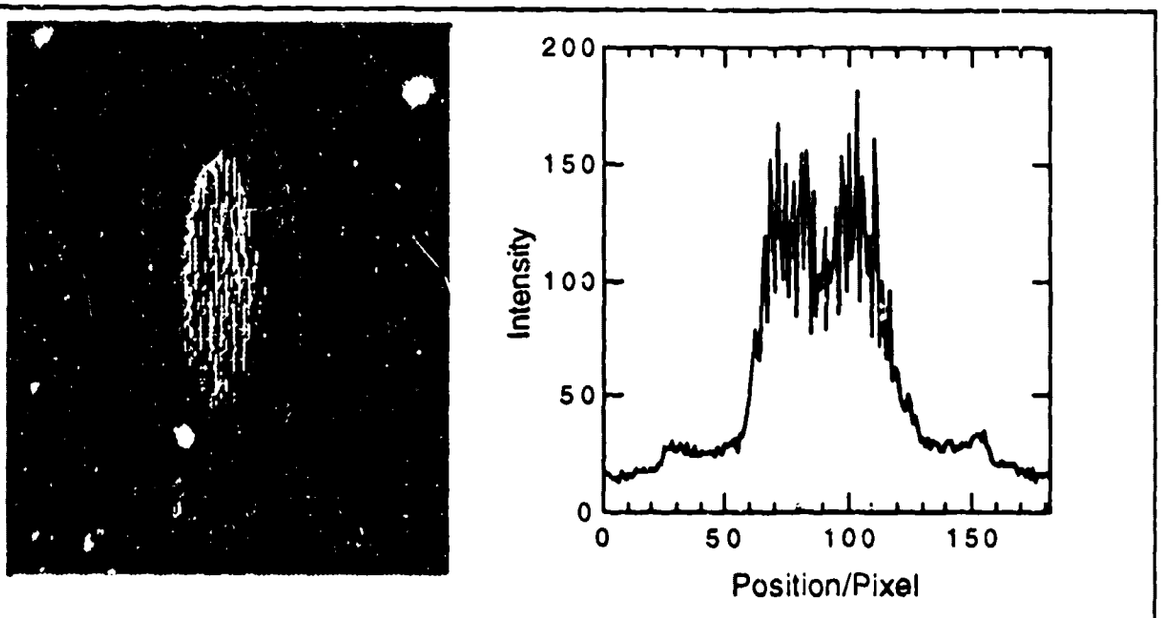

Figure 3. Left side shows an optical micrograph of a laser irradiated spot (≈1000 shots, 7 μJ/shot) for a sample consisting of 20 Å Cu on Si (110). The right side shows intensity as a function of position, for a cut across the center of the spot; in this case the interpeak spacing ≈ 2-3 pixels = 1 μm.

Another aspect of the laser irradiated spots is shown in Figure 3; an interference pattern is often observed in the center of spot, with lines parallel to the direction of propagation of the laser beam. As shown on the right side of Fig. 3, the spacing between lines is ≈1 μm. These patterns were found to be independent of samples orientation, and only weakly dependent on laser polarization (strongest patterns were observed for p-polarization).

3.3 Polarization Dependence.

Figure 4 illustrates the dependence of copper ion signals as a function of polarization of the incident laser light. After analysis with the rough surfaces of high purity copper and the stainless steel SRM were completed, the high purity copper and stainless steel SRM were polished to produce mirror-like finishes similar to the thin copper films on Si (100).

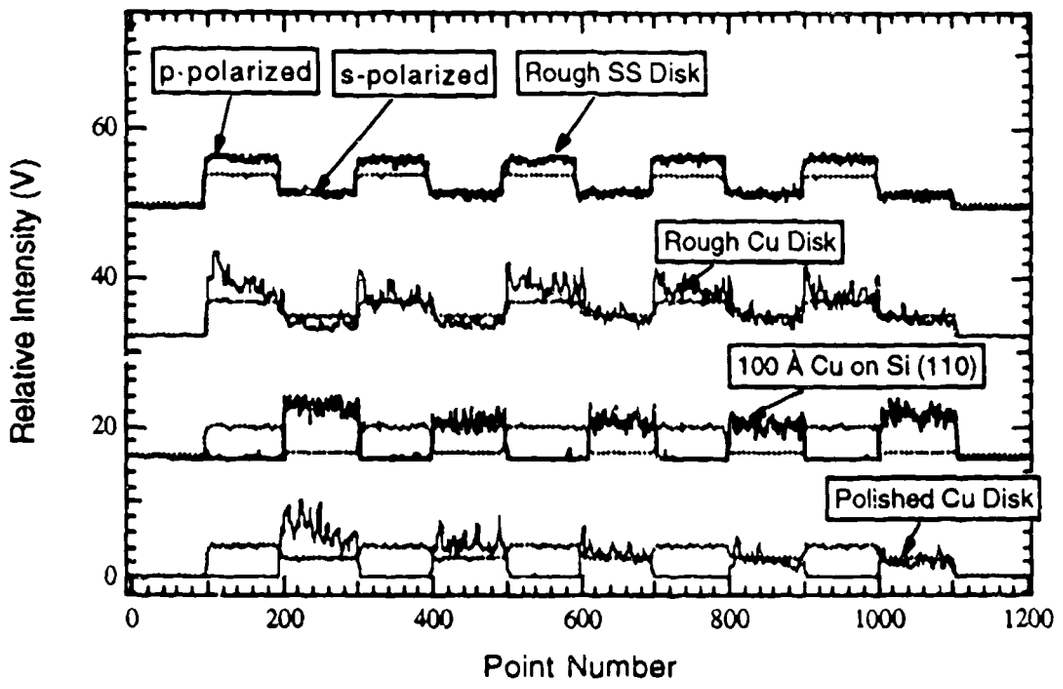

Figure 4. For each sample, we show modulation of the reflected laser beam (dotted line) with polarization modulation, and also the modulation of the copper ion signal (solid line) from the sample in question. The polarization is indicated in the uppermost trace, and is the same for each data set.

The most obvious finding form the data concerns the responses of smooth and rough surfaces; the polarization dependencies for these surfaces are opposed to one another. Whereas smooth surfaces produce a maximum signal for s-polarized light, the rough surfaces produce the maximum signal for p-polarized light. This, despite the fact that the reflected intensities follow the same pattern for both smooth and rough surfaces; p-polarized light is reflected to a greater extent than is s-polarized light. The differences in reflected intensities can be rationalized fairly easily from simple optical physics. The differences in RLA signals are less easily interpretable, and are still under study.

4. Applications

4.1 Spectroscopy

We show here the RLA spectra of Fe atoms ablated at very low fluence from a bulk Re target (70 ppm Fe in rhenium)[17]. Fig. 5 shows the 2+1 multiphoton ionization spectrum of ^{56}Fe detected by RLA. We observe two-photon $\Delta J=0$ transitions from the a^5D ground term to the e^5D excited term near 44640 cm^{-1}. Also shown in Fig. 5 is the $e^5F \leftarrow a^5F$ two-photon transition from the first excited term near ~1 eV. Each of these multiplets spans a wavelength range of <1 nm, yielding essentially constant dye laser power across the multiplet. The $J''=3 \rightarrow J'=3$ and $J''=5 \rightarrow J'=5$ transitions are much stronger than the other lines in this multiplet due to near resonances with the z^5F^o term (detunings of 182 cm^{-1} and 92 cm^{-1}, respectively).

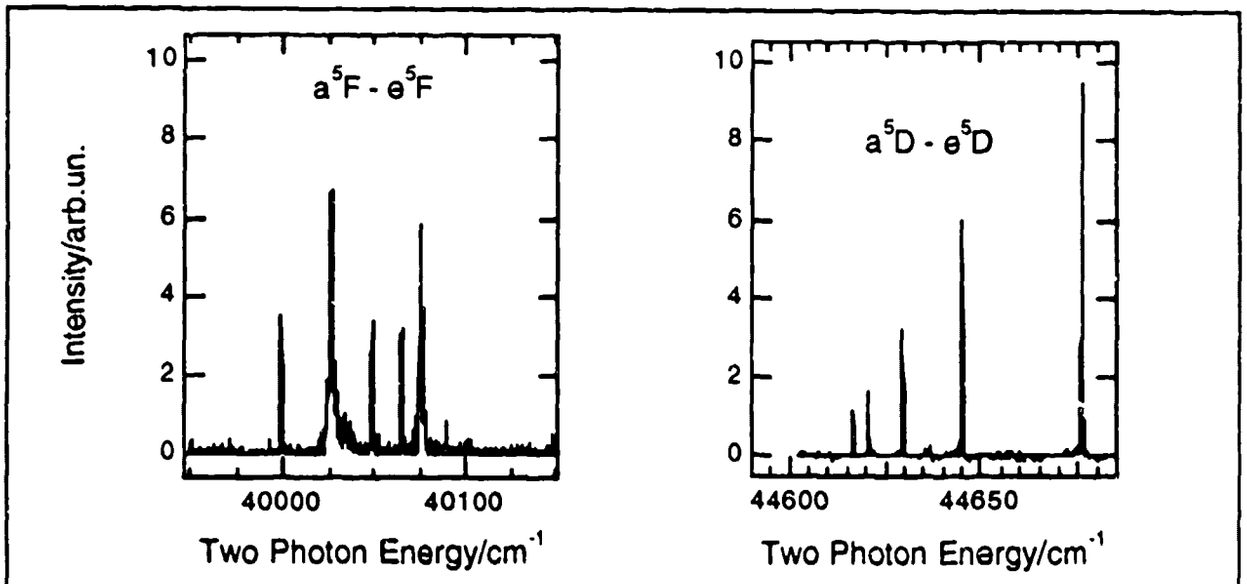

Figure 5 depicts two fine structure manifolds ($\Delta J=0$ transitions) of iron obtained by RLA of iron in a high purity (99.97%) rhenium sample.

Transition intensities can be calculated using second order perturbation theory. We obtain good agreement between experimental and calculated intensities. A fit of the experimental intensities yields a temperature of 1100 ± 200 K for Fe ablation from Re, showing that this spectroscopy can be a useful internal thermometer.

4.2 Thin Film Analysis.

We have recently explored the application of RLA for thin film analysis. With a few notable exceptions, [19,20] most previous studies of laser ablation have produced craters or pits far too deep for analysis of thin films and multilayer structures[21]. Initial experiments described here

involve RLA of copper from SI (110) wafers overcoated with 20 ± 6 Á of Cu. These samples afford the opportunity to quantify material removal under well defined conditions. Figure 6 shows several results from this effort. In the left figure, the copper signal (at constant laser intensity) is found to rise with the rising laser (photodiode) intensity, decrease slowly for several thousand shots, and then end abruptly at channel # 500, corresponding to ≈15,000 laser shots. A nonresonant (potassium) signal is seen to occur largely at the rising and falling edges of the copper signal.

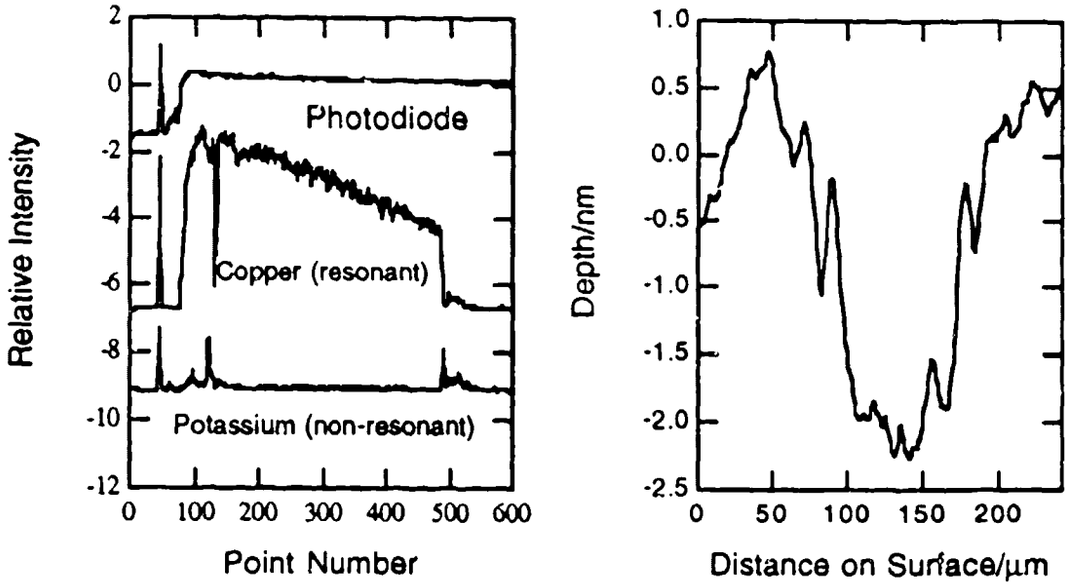

Figure 6. On the left, is displayed laser, copper and potassium signals as a function of irradiation (30 laser shots/point @ 7μJ, $1x10^{-5}$ cm^2) for a sample consisting of 20Á Cu on Si (110). On the right is a profile of the laser spot, obtained with a surface profilimeter.

We believe that the falling edge of the copper signal corresponds to removal of the thin copper film. The transient potassium signals at the rising and falling edges of the copper signal suggest that potassium may be preferential segregating to the interfaces. The right side of figure 6 shows a surface profile of the laser spot, obtained with a interferemetric profilimeter. At the bottom of the pit, the depth of the crater is ≈25 Á, in agreement with the supposition that the falling copper signal corresponds complete removal of the copper film. The slight rises on either side of the crater may be due to redeposition[22] of ablated material. This data suggests that the removal rate under these conditions is ≈0.001 Á/shot.

4.3 Ion Generation for the Ion Trap Mass Spectrometer.

We have also explored the use of RLA as an ion source for the analysis of inorganic materials in a quadrupole ion trap mass spectrometer (ITMS). One of the significant

advantages accruing to the use of RLA as an ion source for the ITMS lies in the selectivity of the process. Ion traps store only a limited number of ions (typically $\leq 10^6$).

Detection of trace components requires that these analytes be produced and trapped in detectable abundances. For components present at less than ppm abundances, this virtually requires a degree of selectivity either in the ionization[23]or trapping process[24]. Using RLA, we nave previously demonstrated[15,17] the detection of components at the sub-ppb level, and selectivities $\geq 10^6$.

Figure 7 shows mass spectra obtained by tuning to the resonant transitions of chromium and iron in a stainless steel sample[16]. Both elements were ionized using "2+1" (photons to resonance + photons to ionize) ionization processes[25]. The left of Fig. 7 depicts the mass spectrum generated by tuning to the 473.3 nm [$3d^5 4d$] e $^7D_3 \leftarrow$ [$3d^5 4s$] a $^7S_3$ 2-photon transition in chromium. The mass spectrum shows primarily the nickel isctopes at m/e=50, (4%), 52 (84%), 53 (10%) and 54 (2%), where the numbers in parentheses indicate natural abundancies. Also observed is a small signal due to the predominant iron isotope at m/e=56. Similarly, the right side of Fig. 7 displays the mass spectrum obtained when the laser is tuned to the 447.97 nm [$3d^6 4s(a\ ^6D_3)5s$] e $^5D_4 \leftarrow$ [$3d^6 4s^2$] e $^5D_3$ 2-photon transition in iron. This spectrum exhibits signal due primarily to iron isctopes at m/e=54 (6%), 56(92%) and 57 (2%), along with some residual signal at m/e=52 from the predominant nickel isotope.

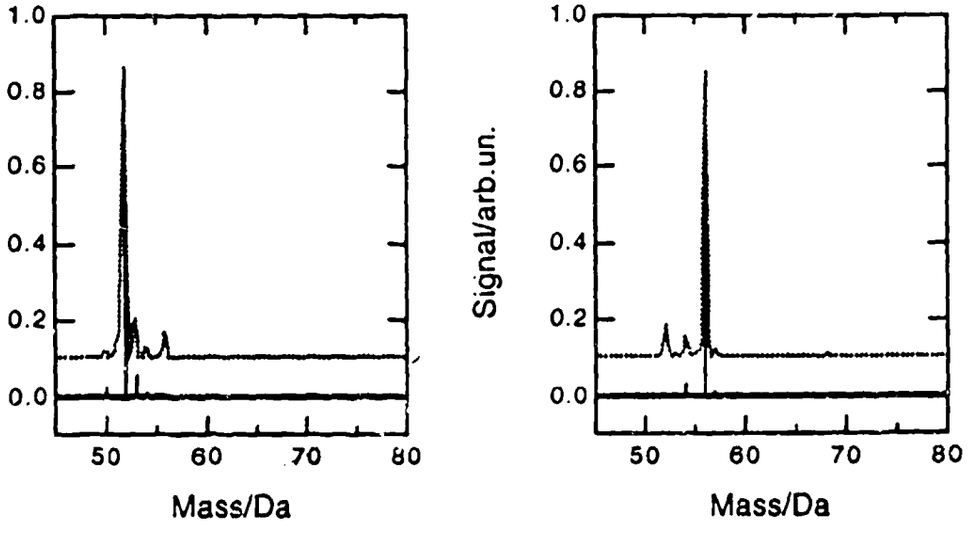

Figure 7. The left panel depicts the RLA mass spectrum of chromium (upper trace) along with a stick spectrum (lower) depicting the normal mass spectrum. The right side shows the RLA mass spectrum and stick spectrum of of iron. Both were obtained in the ITMS.

Some signal from the nonresonant component is also seen in both spectra. The selectivity of the ionization process, while not optimized in these experiments, will allow for the detection of trace components in complex mixtures without the difficulties associated with generating a large excess of matrix ions. The use of a single laser for both the evaporation and ionization processes greatly reduces the complexity relative to separate evaporation (by sputtering or laser ablation) and selective ionization steps.

5. Conclusions

From the work done here[15], and elsewhere[12], a qualitative understanding of the processes and mechanisms involved in RLA is beginning to emerge. It is clear that production of ions is a high (photon) order process, so that precise controal of intensity is essential. Polarization effects are significant, and not yet well understood. The use of non-resonant ionization as an internal calibrant may allow for semi-quantitative analysis.

In the area of new applications, we have shown the ability to perform spectroscpy on trace components, and to determine temperatures from electronic spectra. We have also demonstrated the potential utility of RLA for the analysis of thin films, and multilayer structures. Lastly, the use RLA as a selective ion source for analysis by ITMS has been demonstrated.

References

1. J. F. Ready, *Effects of High-Power Laser Radiation*, 1st ed. (Academic Press, New York, 1971).
2. K. Dittrich and R. Wennrich, *Prog. Anal. At. Spectrosc.* **7,** 139-98 (1984).
3. L. Moenke-Blankenburg, *Laser Microanalysis* (John Wiley & Sons, New York, 1989).
4. L. J. Radziemski and D. A. Cremers, *Laser-Induced Plasma and Applications* (Marcel Dekker, New York, 1989).
5. Y. I. Lee and J. Sneddon, *Analyst* **119(7),** 1441-3 (1994).
6. S. S. Alimpiev, M. E. Belov, and S. M. Nikiforov, *Anal. Chem.* **65,** 3194-8 (1993).
7. M. L. Alexander, P. H. Hemberger, M. E. Cisper, and N. S. Nogar, *Anal. Chem.* **65,** 1609-14 (1993).
8. P. F. Greenwood, G. D. Willett, and M. A. Wilson, *Org. Mass Spectrom.* **28,** 831-40 (1993).
9. P. T. McCombes, I. S. Borthwick, R. Jennings, A. P. Land, K. W. D. Ledingham, R. P. Singhal, and M. Towrie, in *Laser photoionization and desorption surface analysis*

techniques., Vol. 1208, edited by N. S. Nogar (SPIE, Los Angles, Ca, USA, 1990), pp. 18-19.

10. C. J. McLean, J. H. Marsh, A. P. Land, A. Clark, R. Jennings, K. W. D. Ledingham, P. T. McCombes, A. Marshall, R. P. Singhal, and M. Towrie, *Int. J. Mass Spectrom. Ion Process* **96,** R1-R7 (1990).

11. L. Wang, I. S. Borthwick, R. Jennings, P. T. McCombes, K. W. D. Ledingham, R. P. Singhal, and C. J. McLean, *Appl. Phys.* **B53,** 34-38 (1991).

12. I. S. Borthwick, K. W. D. Ledingham, and R. P. Singhal, *Spectrochim. Acta* **47B,** 1259-65 (1992).

13. K. W. D. Ledingham, J. S. Borthwick, and R. P. Singhal, *Surf. Interface Anal* **18,** 576-8 (1992).

14. L. Wang, K. W. D. Ledingham, C. J. McLean, and R. P. Singhal, *Appl. Phys.* **B54,** 71-75 (1992).

15. G. C. Eiden, J. E. Anderson, and N. S. Nogar, *The Microchemical Journal* **In press** (1994).

16. A. W. Garrett, P. H. Hemberger, and N. S. Nogar, *Spectrochimica Acta* **submitted** (1995).

17. G. C. Eiden and N. S. Nogar, *Chem. Phys. Lett.* **226,** 509 (1994).

18. G. C. Eiden, M. E. Cisper, M. L. Alexander, P. H. Hemberger, and N. S. Nogar, *J. Am. Soc. Mass Spec.* **4,** 706-709 (1993).

19. T. Gilbert, B. Dubreuil, M. F. Barthe, and J. L. Debrun, *J. Appl. Phys.* **74,** 3506-13 (1993).

20. O. L. Bourne, D. A. Hart, D. M. Rayner, and P. A. Hackett, *J. Vac. Sci. Technol., B* **11,** 556-61 (1993).

21. T.-Y. Hung and C.-S. Su, *Rev. Sci. Instrum.* **63,** 5299-5305 (1992).

22. R. Kelly, *J. Chem. Phys.* **92,** 5047-56 (1990).

23. C. M. Miller, N. S. Nogar, A. J. Gancarz, and W. R. Shields, *Anal. Chem.* **54,** 2377-8 (1982).

24. A. W. Garrett, M. E. Cisper, N. S. Nogar, and P. H. Hemberger, *Rapid Commun. Mass Spectrom* **8,** 174-8 (1994).

25. E. C. Apel, J. E. Anderson, R. C. Estler, N. S. Nogar, and C. M. Miller, *Appl. Opt.* **26,** 1045-50 (1987).